RESEARCH ARTICLE

Thermally Drawn Multi-material Fibers Based on Polymer Nanocomposite for Continuous Temperature Sensing

Woo Mi Ryu[1] · Yunheum Lee[1] · Yeonzu Son[2] · Geonho Park[3] · Seongjun Park[1,2,4,5]

Abstract

With increasing personalized healthcare, fiber-based wearable temperature sensors that can be incorporated into textiles have attracted more attention in the field of wearable electronics. Here, we present a flexible, well-passivated, polymer–nanocomposite–based fiber temperature sensor fabricated by a thermal drawing process of multiple materials. We engineered a preform to optimize material processability and sensor performance by considering the rheological and functional properties of the preform materials. The fiber temperature sensor consisted of a temperature-sensing core made from a conductive polymer composite of thermoplastic polylactic acid, a conductive carbon filler, reduced graphene oxide, and a highly flexible linear low-density polyethylene passivation layer. Our fiber temperature sensor exhibited adequate sensitivity ($-0.285\%/°C$) within a temperature range of 25–45 °C with rapid response and recovery times of 11.6 and 14.8 s, respectively. In addition, it demonstrated a consistent and reliable temperature response under repeated mechanical and chemical stresses, which satisfied the requirements for the long-term application of wearable fiber sensors. Furthermore, the fiber temperature sensor sewn onto a daily cloth and hand glove exhibited a highly stable performance in response to body temperature changes and temperature detection by touch. These results indicate the great potential of this sensor for applications in wearable, electronic skin, and other biomedical devices.

Woo Mi Ryu, Yunheum Lee, and Yeonzu Son have contributed equally to the work.

✉ Seongjun Park
spark19@kaist.ac.kr

1 Department of Bio and Brain Engineering, Korea Advanced Institute of Science and Technology (KAIST), Daejeon 34141, South Korea

2 Program of Brain and Cognitive Engineering, Korea Advanced Institute of Science and Technology (KAIST), Daejeon 34141, South Korea

3 Department of Chemical and Biomolecular Engineering, Korea Advanced Institute of Science and Technology (KAIST), Daejeon 34141, South Korea

4 KAIST Institute for NanoCentury, Korea Advanced Institute of Science and Technology (KAIST), Daejeon 34141, South Korea

5 KAIST Institute for Health Science and Technology, Korea Advanced Institute of Science and Technology (KAIST), Daejeon 34141, South Korea

Introduction

The recent surge of interest in personalized healthcare, in conjunction with the advances in micro/nanofabrication technologies, has led to the development of wearable devices with continuous and real-time monitoring capacity [1–3]. Wearable devices can detect biological signals directly from the skin. These flexible, lightweight, biocompatible, and highly sensitive electronic devices can detect various signals, including oxygen levels, blood glucose concentration, heart rate, body temperature, electrocardiograms [4–7], electroencephalograms [8, 9], electrooculograms [10–12], and electromyograms [13, 14]. Among these biological readouts, body temperature is a critical indicator of an individual's health status, such as infection [15, 16] and cardiovascular conditions [17]. Various wearable thermal sensors based on ultrathin substrates have recently been reported [18–21]. These sensors exhibit high flexibility and sensitivity, allowing real-time monitoring of body temperature. However, their long-term applications have been limited due to skin

irritation from the substrate and the need of additional fixation materials for conformal contact. To address such limitations, fiber-based thermal sensors have become prominent substitutes that can be incorporated into daily wear. Various fabrication methods, such as solution coating, spinning, and in situ polymerization, have been proposed for developing fiber-based thermal sensors [22–26]. However, these methods have limitations such as low production efficiencies and a lack of physical durability and structural stability of the resulting fibers.

To overcome this limitation, the thermal drawing process (TDP) was introduced as an emerging manufacturing technology for developing fiber-based devices [27–30]. TDP is a conventional production method that was initially used to manufacture optical glass fibers. In TDP, a macroscopic template, called a preform, is heated in a furnace of a drawing tower and elongated with a capstan to be scaled down into a several-hundred-meter-long micro-sized fibers, preserving the cross-sectional architecture [31, 32]. In addition, TDP can be used in a broad range of material selections, from polymers to metals, and facilitate the co-drawing of multiple materials [28, 33–35]. The advantages of TDP make it a promising technique for producing flexible fiber temperature sensors based on soft materials.

A thermally drawn thermal-sensing fiber composed of chalcogenide glass, tin alloy, and polysulfone has been developed [33]. However, the high elastic modulus of the metal and semiconductor in the fiber hampered its practical wearable applications owing to their lack of flexibility. To address this limitation, conductive carbon fillers and polymer composites with distinct properties depending on the type of nanofillers, such as carbon nanotubes [36–38], graphene [39, 40], graphene oxide [41], and reduced graphene oxide (rGO), have been introduced [42, 43]. In particular, rGO possesses a unique two-dimensional and porous structure, which imparts remarkable physical and chemical properties, such as a low percolation threshold [44, 45], relatively high conductivity [46], temperature-sensing property [47], and a large surface area [48]. Furthermore, the large surface area of rGO allows it to interact extensively with the surrounding matrix, making it an attractive option for the development of advanced polymeric composites for various applications, including energy storage [42, 49] and sensing [50, 51].

Herein, we introduced a flexible, well-passivated, polymer–nanocomposite–fiber temperature sensor fabricated using a simple, highly scalable, and cost-efficient TDP. By harnessing the advantages of the TDP, we manufactured polymer nanocomposite fibers from a multi-material preform which consisted of three layers. The innermost part was a temperature-sensing core which consisted of a graphene-based carbon filler with temperature-dependent resistance, rGO, and the thermoplastic biocompatible polymer

polylactic acid (PLA). The outer layer consisted of linear low-density polyethylene (LLDPE), which provided flexible passivation for the mechanical and chemical durability of the fiber temperature sensor. Finally, the outermost sacrificial polystyrene (PS) cladding enabled steady and continuous thermal drawing of the preform into the fiber. Our fiber sensor exhibited adequate sensitivity of $-0.285\%/°C$ with rapid response and recovery times of 11.6 and 14.8 s, respectively, at 25–45 °C. The sensor withstood various stresses, such as mechanical deformation and common solvent exposure, which are essential for long-term applications. Moreover, in practical applications, the fiber temperature sensor exhibited stable and reliable responses to temperature changes, revealing its great potential as a polymer-nanocomposite wearable sensor in the e-healthcare field.

Experimental Section

Materials

PLA (ME3463100) and rGO (rGO-V50) were purchased from Goodfellow Cambridge Ltd. and Standard Graphene, respectively. PS rod (8720K37) was acquired from McMaster-Carr. LLDPE (428,078) was obtained from Merck. Chloroform (2548–4100) and cyclohexane (2606–4404) were purchased from Daejung Chemicals & Metals.

Preform Fabrication and Rheological Analysis of the Conductive Polymer Composite

The flexible polymer–nanocomposite–fiber temperature sensor was produced from the thermal drawing of a macroscopic preform consisting of an rGO and PLA composite (rGO/PLA) temperature-sensing core, an LLDPE passivation layer, and a PS sacrificial layer. The conductive composite sensing core was prepared using the solvent casting method. rGO was first dispersed in chloroform using an ultrasonic bath sonicator for 1 h. Next, PLA granules were added to the rGO dispersion and completely dissolved overnight on a 40 °C hotplate at a stirring rate of 500 rpm. The well-dispersed rGO/PLA suspension was cast on a poly(tetrafluoroethylene)-lined stainless dish and dried overnight to evaporate the chloroform completely. The rGO/PLA film was then shaped into a rod with a diameter of 7–8 mm on a 210 °C hotplate. Next, the conductive composite core was tightly wrapped with hot-pressed LLDPE film with a 150–200 μm thickness. The temperature-sensing core and passivation layer were consolidated using a heat gun and placed in a drilled reservoir of the PS rod to complete the multi-layered preform.

Rheological measurements of the preform materials were performed using a rheometer (Anton Paar, MCR 302). The

polymer samples were prepared in 1-mm-thick disks with a diameter that matched that of the rheometer plate. The samples were heated at 200 °C for 30 min, and contact with the plate was achieved by applying a force set at 0 N. When the temperature of the plate decreased from 155 °C to 125 °C at a rate of 1 °C/min, 0.1% strain was applied to the sample at an angular frequency of 0.03 rad/s.

TDP

Our fiber temperature sensor was fabricated via the TDP using a custom-built fiber drawing tower (Fig. S1). The multi-layered macroscopic preform was placed in the furnace of the tower and preheated at 130 °C for 10 min. After preheating, the furnace temperature was increased to 150 °C until the macroscopic preform was sufficiently softened to be elongated. Once the fiber began to draw from the preform at a capstan pulling rate of 0.3 m/min, the furnace temperature and preform feeding rate were set and maintained at 135 °C and 1 mm/min, respectively. Finally, a thermally drawn flexible polymer–nanocomposite–fiber temperature sensor was fabricated after chemically etching the sacrificial PS layer. Prior to etching, both ends of the drawn fiber were covered with epoxy to prevent solvent penetration into the temperature-sensing core. The well-encapsulated fiber was immersed overnight in cyclohexane on a shaker at a shaking rate of 100 rpm.

Measurements and Characterization

The performance of the fiber temperature sensor was evaluated by measuring the electrical resistance of the fiber sensor using a source meter unit (2450, Keithley). The electrical resistance was measured in the voltage bias mode with the parameters set at a voltage level of 1 V and a current limit of 0.1 mA. The temperature applied to the fiber sensor was controlled using a hot plate (MSH-20D, DAIHAN Scientific). A handheld data logger thermometer (HH378 Data Logger, Omega) was placed adjacent to the fiber temperature sensor to confirm and log the actual temperature applied to the sensor.

The mechanical properties of the fiber sensor were tested using a universal testing machine (Ametek, LS1) with a 10 N load cell. The stretching rate was kept constant at 2 min^{-1}. To estimate the thermal conductivity, thermal diffusivity was measured using a laser flash apparatus (NETZSCH, LFA 467) at a heating rate of 10 °C/min. The heat capacity was obtained using differential scanning calorimetry (NETZSCH, DSC 214 Polyma), with a heating rate of 10 °C/min and a nitrogen purge. The material density was measured using a helium gas pycnometer (Micromeritics, AccuPyc II 1340).

For the measurements, both ends of the rGO/PLA temperature-sensing core of the fiber temperature sensor were exposed and connected to a copper wire using silver paste (ELCOAT P–100, Chemical Aerosol Network System). The wired fiber connections were secured with a thin layer of epoxy. To apply the temperature evenly and instantly, the wired fiber temperature sensor was fixed on a 2-mm-thick aluminum sheet, which made homogeneous contact with the hotplate.

The functional lifespan and performance of the fiber sensor were evaluated using halogen lamp cyclic, mechanical deformation, spill, humidity, and machine-washing tests. The halogen lamp cyclic test was performed by turning a 35 W halogen lamp controlled automatically by Arduino on and off for 20 s at 5 cm above the fiber temperature sensor. The mechanical deformation test was conducted by repetitively bending the fiber sensor at designated angles and bending radii. The spill test was performed by immersing the fiber sensor in 300 mL of detergent, ethyl alcohol, and acetone for 30 min and drying it completely overnight. After each test, the temperature-dependent resistance of the fiber temperature sensor was measured to evaluate its performance stability. The humidity test was conducted by increasing the relative humidity in the chamber and measuring the resistance of the fiber sensor in the chamber in real-time. The relative humidity in the chamber was monitored using a humidity sensor (TM-305U, TENMARS). The machine-washing test was performed by fully immersing the fiber temperature sensor in a 500 mL water bath at 40 °C and 1200 rpm for 30 min [52]. The electrical resistance of the fiber temperature sensor was measured after complete drying overnight.

Results and Discussion

Preform Preparation and TDP

The entire thermally drawn fiber fabrication process is illustrated in Fig. 1a. We utilized thermal drawing, an adaptable process for the mass production of our fiber sensor on a kilometer-long industrial scale, using a thermal drawing tower (Fig. S1). Owing to the nature of the TDP, we could preserve the cross-sectional geometry while adjusting the radial scale by controlling the feed and capstan speeds. The theoretical diameter of the fiber was calculated using Eq. (1).

$$R_{\text{fiber}} = \sqrt{\frac{V_{\text{feed}}}{V_{\text{capstan}}}} \times R_{\text{preform}} \tag{1}$$

In this equation, R_{fiber} and R_{preform} are the radii of the fiber and preform, respectively, and V_{feed} and V_{capstan} are the speeds of the feed and capstan, respectively.
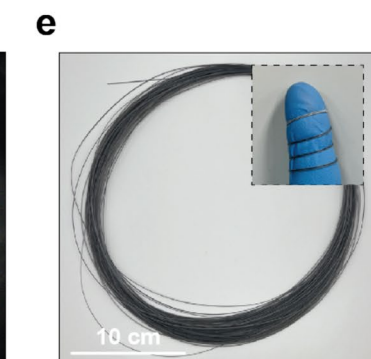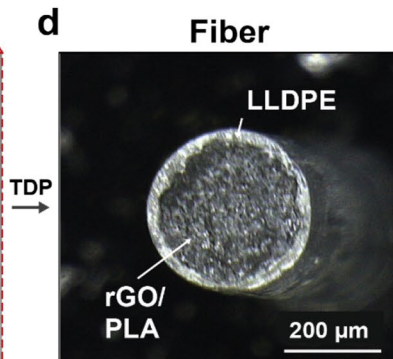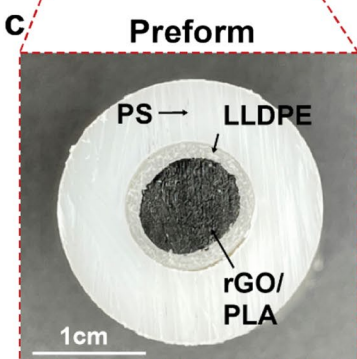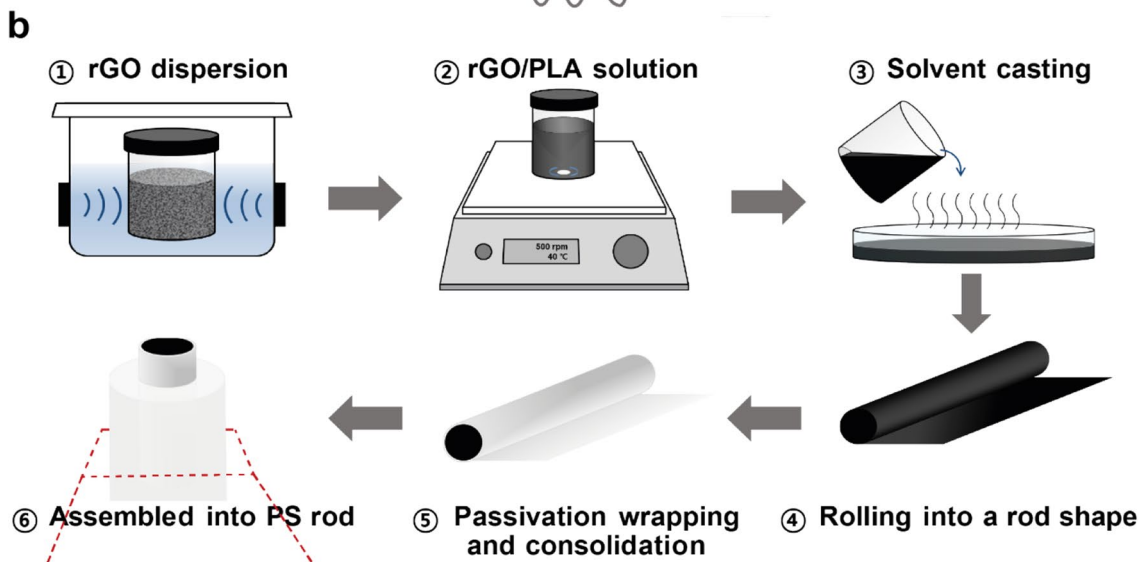
$$R_{fiber} = \sqrt{\frac{V_{feed}}{V_{capstan}}} \times R_{preform}$$

Our fiber temperature sensor was heated and drawn from a multi-material preform which consisted of three parts. The innermost temperature-sensing part of the preform was composed of rGO and PLA. rGO yields differential conductivity in response to the external temperature, whereas PLA is a thermoplastic polymer commonly used for various thermal processes. In addition to the temperature-sensing core, LLDPE was used as a passivation layer. The outermost layer comprised a sacrificial PS layer that allowed a continuous and steady TDP while leaving the inner sensing parts intact.

Figure 1b illustrates the general preform preparation process. Briefly, the temperature-sensing core was prepared by solvent-casting the composite comprising the conductive carbon filler rGO and the thermoplastic polymer PLA. After completely evaporating the solvent, the casted rGO/PLA film was formed into a rod shape and then wrapped with LLDPE for additional mechanical and chemical durability. Next, we assembled the bilayer using the sacrificial PS cladding to complete the macroscopic preform (Fig. 1c), which was then heated and elongated in the thermal drawing tower. The sacrificial PS layer on the resultant fiber was removed using cyclohexane (Fig. 1d). Consequently, a several-hundred-meter-long microscopic fiber (Fig. 1e), whose diameter could be easily adjusted by altering the drawing parameters, was obtained. The fiber diameter was miniaturized from 20- to 127-fold while preserving the cross-sectional multi-layer structure (Fig. S2). For our experiments, we used the fiber with an average pre-etching diameter of 770 ± 47.33 μm and an average post-etching diameter of 240.2 ± 54.85 μm to optimize the flexibility and functionality of the fiber sensor (Fig. S3).

To achieve both stable thermal drawing and retention of the original cross-sectional geometry, the multi-material preform must be viscoelastic. It should also be heated above the highest glass transition temperature (T_g), near the melting temperature (T_m) of the constituent materials before the elongation process [32, 53]. As the preform is heated above the T_g, the materials transition from an elastic to a viscous state, where their stiff solid-like (elastic) behavior changes to a soft liquid-like (viscous) behavior, allowing for stable thermal drawing [54, 55]. Accordingly, the rheological behavior of the conductive polymer composite at the thermal drawing temperature can affect the stability of the drawing process. Thus, we performed rheological studies to identify the drawable rGO concentration range in the rGO/PLA. We prepared rGO/PLA with six different rGO weight percentages and measured their complex viscosities at between the T_g and T_m of PLA (Table 1) to ensure that the composite can undergo TDP. In this temperature range, elevated rGO concentrations resulted in an increased complex viscosity (Fig. 2a). The rGO/PLA with an rGO concentration just above 1.3 wt% had a crossover point of storage and loss modulus at 150 °C (Fig. 2b). This implies that the composite with higher rGO content (above 1.3 wt%) exhibited a more dominant elastic behavior than the viscous behavior as the rGO sheets hindered the chain mobility of PLA [54, 56]. Therefore, the rGO concentration was maintained below 1.3 wt% in the conductive polymer composite for the stable thermal drawing.

Next, to stabilize the TDP, we engineered the outer layers of the fiber temperature sensor preform. Lightweight LLDPE was selected as the passivation layer, allowing the fiber to be more flexible and mechanically and chemically durable. However, because of its low T_m (Table 1), LLDPE had a significantly lower complex viscosity at the temperature at which the rGO/PLA could be thermally processed (Fig. 2c). This resulted in a discrepancy between their fluidic behaviors at the drawing temperature, leading to poor retention of the cross-sectional geometry. To address this challenge, we added a PS cladding layer with a more compatible rheological property with rGO/PLA than LLDPE. The higher complex viscosity of PS at all applied temperatures enabled the maintenance of the multi-layer structure of the preform, supporting continuous TDP (Fig. 2c).

Subsequently, we performed functional evaluations of the thermally drawn fibers using sensing cores with different rGO concentrations. When measuring the electrical conductivity of thermally drawn fibers with varying rGO concentrations, we observed that the rGO sheets had not yet formed interconnected networks within the elongated fibers at a low concentration (0.5 wt%), resulting in a conductivity equal to that of the bare PLA polymer film (Fig. 2d). The rGO network underwent a rapid transition as the rGO concentration increased, establishing a percolation network in which the flow of charge carriers between the rGO sheets increased dramatically [18]. At concentrations above 1.3 wt%, the conductivity of the fibers leveled off, indicating maximum fiber conductivity [44]. Considering both processability and functionality, we concluded that the fiber sensor with the sensing core composed of 1.3 wt% rGO/PLA was optimal for the subsequent experiments because of its stable drawability and high electrical conductivity of 1.45 mS/cm. The intrinsic properties of the fiber sensor were further investigated to ensure its applicability in wearable devices.

Table 1 Thermal properties of the materials constituting the preform of the polymer–nanocomposite–fiber temperature sensor [57]

Materials	Glass transition temperature (°C)	Melting temperature (°C)
PLA	63	178
LLDPE	− 35	125
PS	80–90	240

We estimated its thermal conductivity within the range of 25–65 °C using the Eq. (2):

$$k = a C_p \rho \tag{2}$$

where a is the thermal diffusivity of rGO/PLA, C_p is the heat capacity, and ρ is the material density (Fig. S4). Based on the stress–strain curve (Fig. S5), the Young's Modulus and tensile strength of our fiber sensor were 1.64 GPa and 28.6 MPa, respectively.

Sensing Performance of the Fiber Temperature Sensor

Next, we evaluated the temperature-sensing performance of our fiber temperature sensor. The general schematics of the electrical resistance measurements are provided in the Supplementary Information (Fig. S6). We chose a temperature range of 25–45 °C, which includes the typical range of human skin temperatures for wearable applications [43].

The functional filler rGO has a negative temperature coefficient of resistance (TCR), which can be ascribed to the electrical conductance of the intra- and inter-sheets of
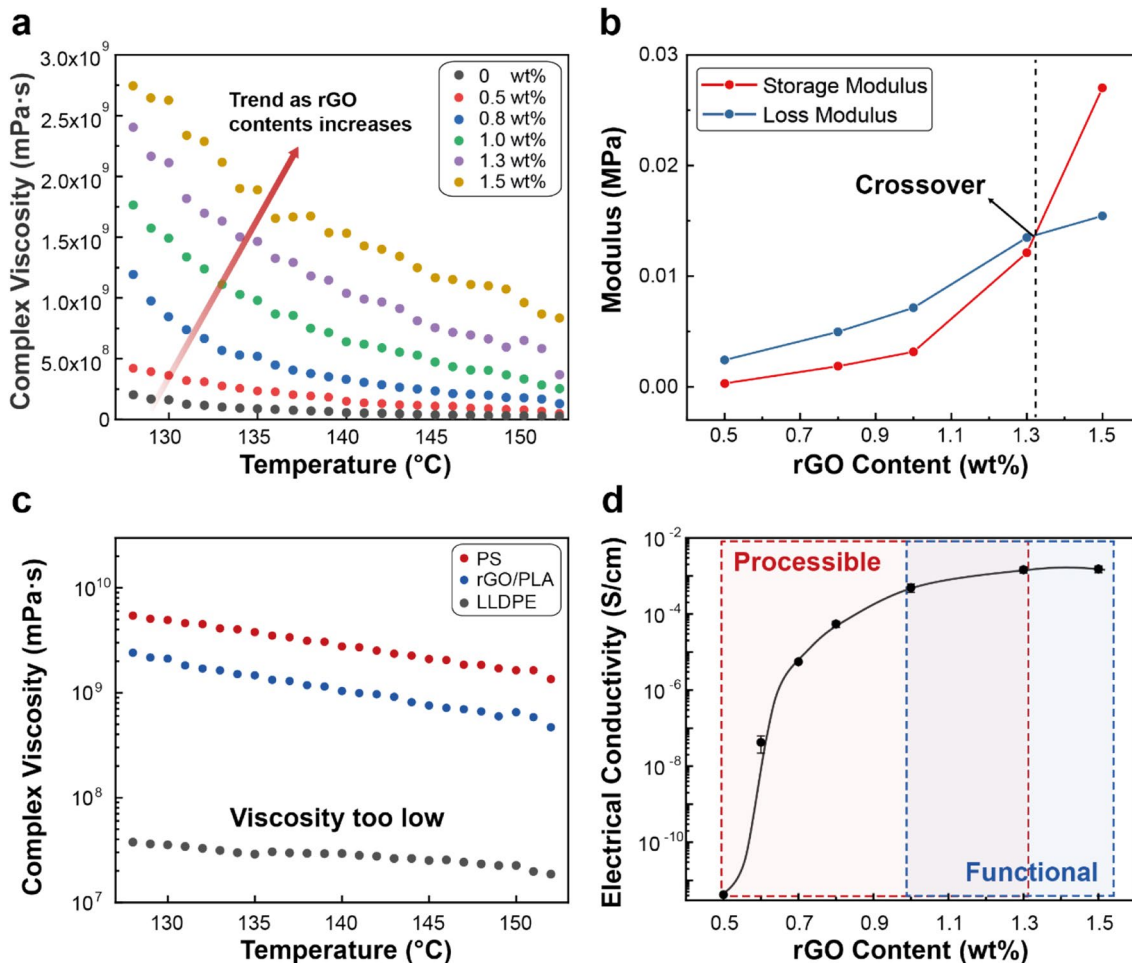

Fig. 2 Fundamental characterization of the preform materials of the polymer–composite–fiber temperature sensor. **a** Complex viscosity of the conductive polymer composites with different rGO weight percentages. **b** Storage and loss moduli of the rGO/PLA with different rGO weight percentages at 150 °C. **c** Complex viscosity of the sensing core, passivation, and sacrificial materials. **d** Electrical conductivity of thermally drawn fibers with different rGO concentrations in the temperature-sensing core at 25 °C

rGO [23]. After the reduction of graphene oxide, residual oxygen-containing functional groups in the rGO sheet create defects in its orbital structure, causing the formation of a bandgap between the valence and conduction bands [47, 58, 59]. Consequently, charge carriers must overcome the potential barrier via hopping to achieve electrical conductivity. The percolation network formed between rGO sheets also contributes to electrical conductivity by establishing the pathway for the flow of charge carriers and demonstrating a tunneling effect [44]. As temperature increases, the probability of hopping and tunneling by thermally activated carriers increases, thereby decreasing resistance. This results in a negative temperature coefficient. The performance was estimated by calculating the TCR using Eq. (3).

$$\text{TCR} = \frac{R_T - R_0}{R_0} \frac{1}{\Delta T} \times 100\% \tag{3}$$

In this equation, R_T and R_0 are the resistances measured across the sensor at the applied and ambient temperatures, respectively, and ΔT is the temperature change [60, 61]. As shown in Fig. 3a, the electrical resistance linearly decreased when the temperature increased from 25 to 45 °C with TCR and R^2 values of -0.285%/°C and 0.999, respectively. The resolution of the fiber temperature sensor with small temperature increments of 0.5 °C maintained its linearity and sensitivity with an R^2 value of 0.996 (Fig. 3b). The performance of the fiber temperature sensor was maintained regardless of the length of the fiber (Fig. 3c), and the temperature reading remained consistent over a long period of time (Fig. 3d). In addition, the fiber temperature sensor showed rapid response and recovery times to touch (11.6 and 14.8 s, respectively) with complete resistance recovery (Fig. 3e).

The thermally drawn temperature sensor exhibited a consistent response during repetitive heating and cooling cycles (Fig. 3f). These results demonstrate that our fiber temperature sensor is reliable and consistent for any length of use and is potentially applicable for continuous and repetitive real-time temperature sensing.

Performance Stability of the Fiber Temperature Sensor

Wearable textile sensors are often exposed to various stresses, such as bending, staining, and washing, which can damage the sensor's functionality (Fig. 4a). Therefore, textile sensors must possess sufficient mechanical and chemical stabilities to achieve high insulating capacity, flexibility, and durability, which are required for everyday applications. We performed various functional evaluations on our fiber temperature sensor to assess its stability and reliability under stress. First, we applied specific and repeated stresses to our fiber sensor. After we performed a thousand heating cycles

using an Arduino-controlled halogen lamp, the performance of our fiber temperature sensor was unaffected as the electrical resistance reliably and linearly reflected the applied temperature, demonstrating the long-term usability of the sensor (Fig. 4b, Fig. S7). Next, we assessed the fiber sensor's mechanical stability by altering the radii of curvature at various folding angles. When we tested the extreme bending angles of 90° and 180° with varying radii of curvature, the temperature response of our fiber sensor remained constant at room temperature (Fig. S8). Furthermore, when we applied a bending angle of 90° at two different radii of curvature (0.5 and 1.5 cm), our fiber temperature sensor demonstrated consistent performance over the selected temperature range (25–45 °C) (Fig. 4c).

To apply an even harsher mechanical deformation, we performed repeated bending cycles on our fiber temperature sensor at a bending angle of 90° and a radius of curvature of 1.5 cm. Even after 100 and 1000 bending cycles, our fiber temperature sensor still reliably responded to the changes in external temperature (Fig. 4d). These results indicate that the flexible polymer–nanocomposite–fiber temperature sensor can withstand various and repeated mechanical deformations while maintaining a reliable and stable performance.

Next, we evaluated the chemical resistance of the fiber temperature sensor. To mimic real-life spillage conditions, we selected the three most common solvents (commercial detergent, ethanol, and acetone) and immersed our fiber temperature sensor in each solvent. Our fiber temperature sensor performed with high consistency at all conditions, with an error range of $\pm 0.18\%$ after chemical exposure (Fig. 4e). In addition, no performance change was observed in the fiber temperature sensor after increasing the relative humidity from 20 to 90% at room temperature (Fig. 4f). Finally, we tested the washability of our fiber sensor by mimicking machine-washing conditions [52]. Briefly, the fiber sensor was fully immersed in a water bath at 40 °C while stirring at 1200 rpm. Even in this harsh condition combining both thermal and mechanical disruption, our fiber temperature sensor still reliably responded to the external temperature, with a $\pm 0.3\%$ error (Fig. 4g). Together, these results demonstrate that our fiber temperature sensor can withstand various chemical damages because the LLDPE passivation layer prevents direct contact of the temperature-sensing core with the outer environments. TDP produced full passivation layer as the process preserves the original structure of the preform and uniformly consolidates all layers throughout the entire length of the drawn micro-fiber during the heating and elongation processes. Table S1 compares overall performance of the sensor developed in this study and those from previous studies, indicating that the performance of our fiber temperature sensor is comparable to that of existing sensors used in various wearable sensor applications.
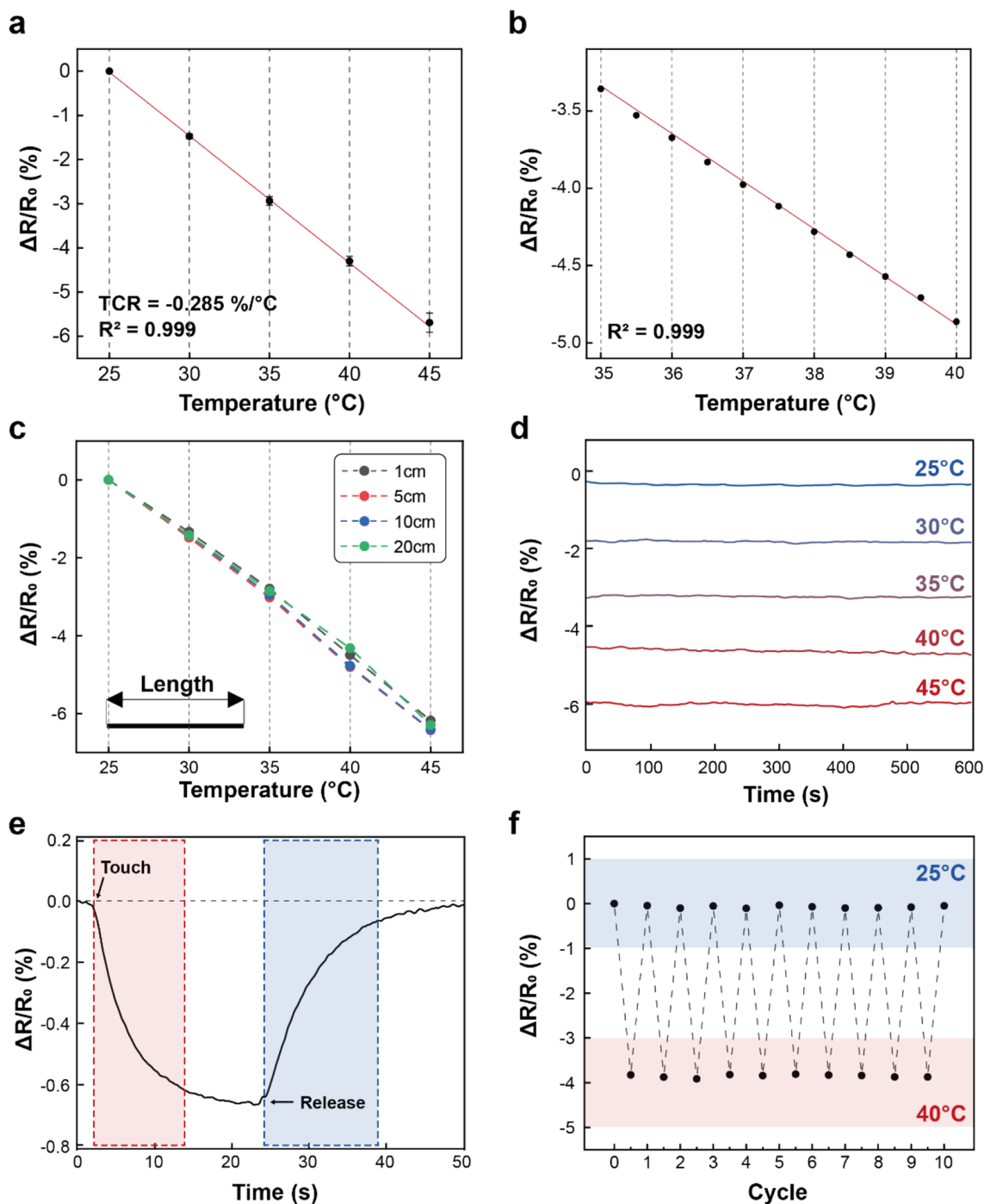
Fig. 3 Performance of the thermally drawn, polymer–nanocomposite–fiber temperature sensor. **a** Resistance response of the fiber sensor to temperature changes from 25 to 45 °C. **b** Resistance response of the fiber sensor to temperature changes with 0.5 °C increments from 35 to 40 °C. **c** Temperature response of the thermally drawn fiber sensor at different lengths. **d** Resistance response of the thermally drawn fiber sensor to constant temperatures for 10 min. **e** Response and recovery time of the fiber sensor to a fingertip touch. **f** Temperature response of the fiber sensor to repetitive cooling and heating cycles from 25 to 40 °C

Applications of the Fiber Temperature Sensor

To test the applicability of the polymer–nanocomposite–fiber temperature sensor in practical situations, we incorporated our fiber into daily clothing. The flexibility and adjustable diameter of the fiber allowed us to weave it into or sew it onto fabric (Fig. 5a). We sewed our fiber temperature sensor onto a shirt to monitor the body
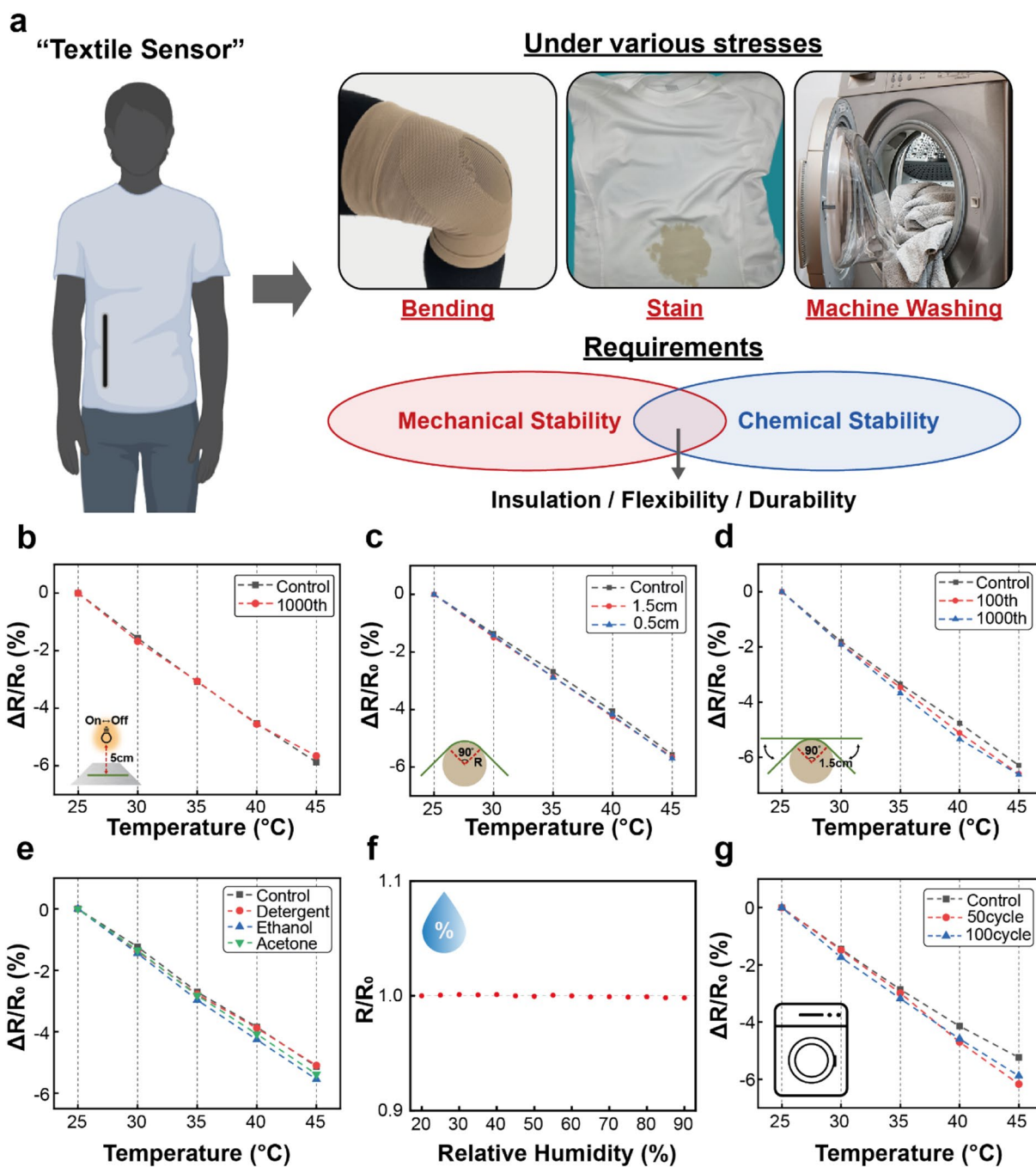
Fig. 4 Performance stability of the thermally drawn, polymer–nanocomposite–fiber temperature sensor under various stress conditions. **a** Schematic illustration of the general requirements of textile sensors. **b** Temperature response of the sensor between 25 and 45 °C after a thousand heating cycles. **c** Resistance response of the fiber sensor bent at a 90° angle with radii of curvature of 1.5 cm and 0.5 cm. **d** Resistance response of the fiber sensor after the 100th and 1000th bending cycles. **e** Temperature response of the fiber sensor after exposure to common chemicals for 30 min. **f** Resistance behavior of the fiber sensor to relative humidity levels between 20% and 90%. **g** Resistance response of the fiber sensor following the 50th and 100th machine-wash test cycles

temperature (Fig. 5b). As soon as the sensor-sewn shirt came in contact with the skin, the electrical resistance of the fiber immediately decreased, indicating a temperature rise. However, during routine activities such as breathing, speaking, and walking, the resistance remained constant, demonstrating that the response was exclusive to temperature change. The resistance completely recovered to the original value when the shirt was removed from the body. For repetitive skin-temperature monitoring, a commercial thermocouple was affixed to the fiber sensor
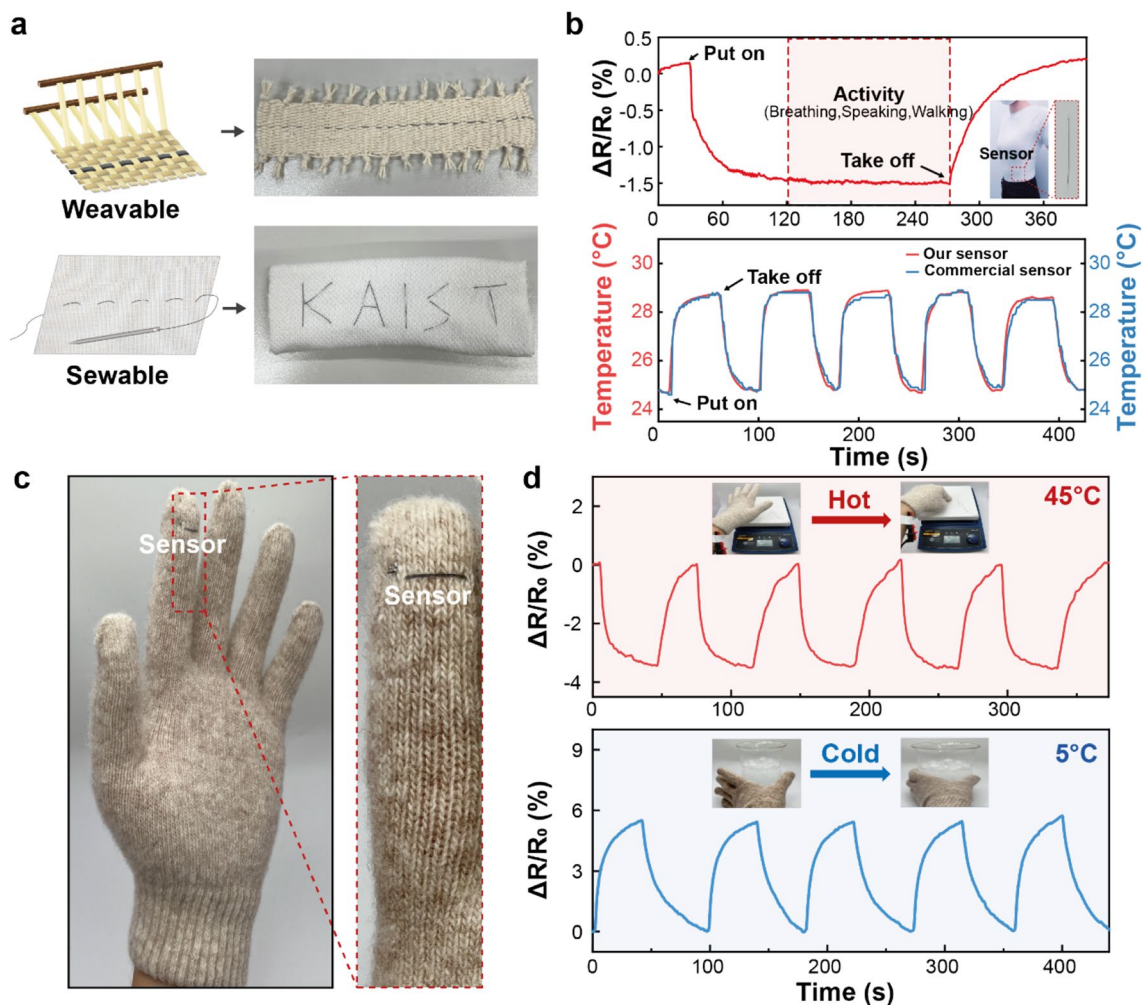
Fig. 5 Wearable applications of the thermally drawn, polymer–nanocomposite–fiber temperature sensor. **a** Illustrations and corresponding photographs of the fiber sensor woven onto a piece of textile (top) and sewn on a headband (bottom). **b** Real-time resistance change of the fiber sensor sewn onto a shirt in response to the skin contact and routine activities (top) and repetitive real-time skin temperature measurements with our fiber sensor and a commercial thermocouple (bottom). **c** Image of the fiber temperature sensor sewn onto the tip of a hand glove. **d** Temperature response of the fiber sensor to repetitive touch on a hot (45 °C) or cold (5 °C) object

to ensure consistency. Compared with the commercial thermocouple, our fiber temperature sensor demonstrated accurate and consistent temperature responses to the skin temperature. Next, we incorporated our fiber temperature sensor into a glove for touch-based temperature detection. We sewed our fiber sensor onto a commercially available glove (Fig. 5c) and measured its response when either a hot (40 °C) or a cold (5 °C) object was touched (Fig. 5d).

The electrical response of the fiber was consistently reproduced without signal delay or degeneration, even with repeated touches. Overall, our thermally drawn, flexible fiber temperature sensor can be incorporated into daily clothing and other practical applications owing to its flexibility and robustness. Additionally, the rapid, consistent, and accurate response of our fiber allowed us to monitor temperature changes in real-time, thereby revealing the utility of our fiber temperature sensor for a wide range of wearable applications.

Conclusions

We developed a well-passivated, polymer–nanocomposite–fiber temperature sensor fabricated via TDP, a facile and economical method of mass production. We engineered the preform materials, especially the conductive polymer composite, to ensure both the processability and functionality of the fiber temperature sensor. Our thermally drawn polymer–fiber temperature sensor demonstrated a sensitive and consistent temperature response in the body temperature range, with rapid response and recovery times. Our highly flexible, durable, and well-passivated

conductive polymer–composite–fiber temperature sensor exhibited consistent temperature responses under repeated mechanical and chemical stresses, indicating its long-term applicability with accurate and stable responses. In practical applications, the fiber temperature sensor woven onto a shirt and a glove demonstrated highly stable and reliable performance, with responses exclusive to the applied temperature. We envision that this highly flexible, durable, and reliable polymer–nanocomposite–fiber temperature sensor fabricated by TDP can be integrated into various electronic healthcare fields, including wearable sensors, electronic skin, and biomedical devices.

Data availability The data that support the findings of this study are available from the corresponding author upon reasonable request.

Declarations

Conflict of Interest The authors declare no conflict of interest.

References

1. Khan Y, Ostfeld AE, Lochner CM, Pierre A, Arias AC. Monitoring of vital signs with flexible and wearable medical devices. *Adv Mater*. **2016**;*28*:4373.

2. Iqbal SMA, Mahgoub I, Du E, Leavitt MA, Asghar W. Advances in healthcare wearable devices. *npj Flex Electron*. **2021**;*5*:9.

3. Li F, Xue H, Lin X, Zhao H, Zhang T. Wearable temperature sensor with high resolution for skin temperature monitoring. *ACS Appl Mater Interfaces*. **2022**;*14*:43844.

4. Coosemans J, Hermans B, Puers R. Integrating wireless ECG monitoring in textiles. *Sens Actuators A Phys*. **2006**;*130–131*:48.

5. Kabiri Ameri S, Ho R, Jang H, Tao L, Wang Y, Wang L, Schnyer DM, Akinwande D, Lu N. Graphene electronic tattoo sensors. *ACS Nano*. **2017**;*11*:7634.

6. Yapici MK, Alkhidir TE. Intelligent medical garments with graphene-functionalized smart-cloth ECG sensors. *Sensors (Basel)*. **2017**;*17*:875.

7. Arquilla K, Webb AK, Anderson AP. Textile electrocardiogram (ECG) electrodes for wearable health monitoring. *Sensors (Basel)*. **2020**;*20*:1013.

8. Lofhede J, Seoane F, Thordstein M. Textile electrodes for EEG recording–a pilot study. *Sensors (Basel)*. **2012**;*12*:16907.

9. Gao KP, Shen GC, Zhao N, Jiang CP, Yang B, Liu JQ. Wearable multifunction sensor for the detection of forehead EEG signal and sweat rate on skin simultaneously. *IEEE Sens J*. **2020**;*20*:10393.

10. Arnin J, Anopas D, Horapong M, Triponyuwasi P, Yamsa-ard T, Iampetch S, Wongsawat Y (eds) (2013) Wireless-based portable EEG-EOG monitoring for real time drowsiness detection. In: 2013 35th annual international conference of the IEEE engineering in medicine and biology society (EMBC). 3–7 July 2013

11. Paul G, Torah R, Beeby S, Tudor J. The development of screen printed conductive networks on textiles for biopotential monitoring applications. *Sens Actuators A Phys*. **2014**;*206*:35.

12. Golparvar AJ, Yapici MK (eds) (2018) Graphene-coated wearable textiles for EOG-based human-computer interaction. In: 2018 IEEE 15th international conference on wearable and implantable body sensor networks (BSN). 4–7 March 2018

13. Sumner B, Mancuso C, Paradiso R (eds) (2013) Performances evaluation of textile electrodes for EMG remote measurements. In: 2013 35th annual international conference of the IEEE engineering in medicine and biology society (EMBC). 3–7 July 2013

14. Pino EJ, Arias Y, Aqueveque P (eds) (2018) Wearable EMG shirt for upper limb training. In: 2018 40th annual international conference of the IEEE engineering in medicine and biology society (EMBC). 18–21 July 2018

15. Kushimoto S, Gando S, Saitoh D, Mayumi T, Ogura H, Fujishima S, Araki T, Ikeda H, Kotani J, Miki Y, Shiraishi S, Suzuki K, Suzuki Y, Takeyama N, Takuma K, Tsuruta R, Yamaguchi Y, Yamashita N, Aikawa N. The impact of body temperature abnormalities on the disease severity and outcome in patients with severe sepsis: an analysis from a multicenter, prospective survey of severe sepsis. *Crit Care*. **2013**;*17*:R271.

16. Yamamoto S, Yamazaki S, Shimizu T, Takeshima T, Fukuma S, Yamamoto Y, Tochitani K, Tsuchido Y, Shinohara K, Fukuhara S. Body temperature at the emergency department as a predictor of mortality in patients with bacterial infection. *Medicine (Baltimore)*. **2016**;*95*: e3628.

17. Reith J, Jørgensen HS, Pedersen PM, Nakayama H, Raaschou HO, Jeppesen LL, Olsen TS. Body temperature in acute stroke: relation to stroke severity, infarct size, mortality, and outcome. *Lancet*. **1996**;*347*:422.

18. Liu Q, Tai H, Yuan Z, Zhou Y, Su Y, Jiang Y. A high-performances flexible temperature sensor composed of polyethyleneimine/reduced graphene oxide bilayer for real-time monitoring. *Adv Mater Technol*. **2019**;*4*:1800594.

19. Dan L, Elias AL. Flexible and stretchable temperature sensors fabricated using solution-processable conductive polymer composites. *Adv Healthc Mater*. **2020**;*9*:e2000380.

20. Wang Y-F, Sekine T, Takeda Y, Yokosawa K, Matsui H, Kumaki D, Shiba T, Nishikawa T, Tokito S. Fully printed PEDOT:PSS-based temperature sensor with high humidity stability for wireless healthcare monitoring. *Sci Rep*. **2020**;*10*:2467.

21. Daus A, Jaikissoon M, Khan AI, Kumar A, Grady RW, Saraswat KC, Pop E. Fast-response flexible temperature sensors with atomically thin molybdenum disulfide. *Nano Lett*. **2022**;*22*:6135.

22. Sibinski M, Jakubowska M, Sloma M. Flexible temperature sensors on fibers. *Sensors (Basel)*. **2010**;*10*:7934.

23. Trung TQ, Le HS, Dang TML, Ju S, Park SY, Lee N-E. Free-standing, fiber-based, wearable temperature sensor with tunable thermal index for healthcare monitoring. *Adv Healthc Mater*. **2018**;*7*:1800074.

24. Wu R, Ma L, Hou C, Meng Z, Guo W, Yu W, Yu R, Hu F, Liu XY. Silk composite electronic textile sensor for high space precision 2D combo temperature-pressure sensing. *Small*. **2019**;*15*: e1901558.

25. Lee J, Kim DW, Chun S, Song JH, Yoo ES, Kim JK, Pang C. Intrinsically strain-insensitive, hyperelastic temperature-sensing

fiber with compressed micro-wrinkles for integrated textronics. *Adv Mater Technol*. **2020**;*5*:2000073.

26. Libanori A, Chen G, Zhao X, Zhou Y, Chen J. Smart textiles for personalized healthcare. *Nat Electron*. **2022**;*5*:142.

27. Lu C, Park S, Richner TJ, Derry A, Brown I, Hou C, Rao S, Kang J, Moritz CT, Fink Y, Anikeeva P. Flexible and stretchable nanowire-coated fibers for optoelectronic probing of spinal cord circuits. *Sci Adv*. **2017**;*3*:e1600955.

28. Park S, Guo Y, Jia X, Choe HK, Grena B, Kang J, Park J, Lu C, Canales A, Chen R, Yim YS, Choi GB, Fink Y, Anikeeva P. One-step optogenetics with multifunctional flexible polymer fibers. *Nat Neurosci*. **2017**;*20*:612.

29. Shahriari D, Loke G, Tafel I, Park S, Chiang PH, Fink Y, Anikeeva P. Scalable fabrication of porous microchannel nerve guidance scaffolds with complex geometries. *Adv Mater*. **2019**;*31*: e1902021.

30. Yan W, Noel G, Loke G, Meiklejohn E, Khudiyev T, Marion J, Rui G, Lin J, Cherston J, Sahasrabudhe A, Wilbert J, Wicaksono I, Hoyt RW, Missakian A, Zhu L, Ma C, Joannopoulos J, Fink Y. Single fibre enables acoustic fabrics via nanometre-scale vibrations. *Nature*. **2022**;*603*:616.

31. Lee J, Llerena Zambrano B, Woo J, Yoon K, Lee T. Recent advances in 1D stretchable electrodes and devices for textile and wearable electronics: materials, fabrications, and applications. *Adv Mater*. **2020**;*32*:e1902532.

32. Loke G, Yan W, Khudiyev T, Noel G, Fink Y. Recent progress and perspectives of thermally drawn multimaterial fiber electronics. *Adv Mater*. **2020**;*32*:1904911.

33. Bayindir M, Abouraddy AF, Arnold J, Joannopoulos JD, Fink Y. Thermal-sensing fiber devices by multimaterial codrawing. *Adv Mater*. **2006**;*18*:845.

34. Grena B, Alayrac J-B, Levy E, Stolyarov AM, Joannopoulos JD, Fink Y. Thermally-drawn fibers with spatially-selective porous domains. *Nat Commun*. **2017**;*8*:364.

35. Kim J, Zhao Y, Yang S, Feng Z, Wang A, Davalos RV, Jia X. Laser machined fiber-based microprobe: application in microscale electroporation. *Adv Fiber Mater*. **2022**;*4*:859.

36. Wu Y, Zhao X, Shang Y, Chang S, Dai L, Cao A. Application-driven carbon nanotube functional materials. *ACS Nano*. **2021**;*15*:7946.

37. Dai H, Thostenson ET. Large-area carbon nanotube-based flexible composites for ultra-wide range pressure sensing and spatial pressure mapping. *ACS Appl Mater Interfaces*. **2019**;*11*:48370.

38. Cai Y, Shen J, Ge G, Zhang Y, Jin W, Huang W, Shao J, Yang J, Dong X. Stretchable Ti3C2Tx MXene/carbon nanotube composite based strain sensor with ultrahigh sensitivity and tunable sensing range. *ACS Nano*. **2018**;*12*:56.

39. Han Z, Wang J, Liu S, Zhang Q, Liu Y, Tan Y, Luo S, Guo F, Ma J, Li P, Ming X, Gao C, Xu Z. Electrospinning of neat graphene nanofibers. *Adv Fiber Mater*. **2022**;*4*:268.

40. Eom W, Lee SH, Shin H, Jeong W, Koh KH, Han TH. Microstructure-controlled polyacrylonitrile/graphene fibers over 1 gigapascal strength. *ACS Nano*. **2021**;*15*:13055.

41. Ming X, Wei A, Liu Y, Peng L, Li P, Wang J, Liu S, Fang W, Wang Z, Peng H, Lin J, Huang H, Han Z, Luo S, Cao M, Wang B, Liu Z, Guo F, Xu Z, Gao C. 2D-topology-seeded graphitization for highly thermally conductive carbon fibers. *Adv Mater*. **2022**;*34*:2201867.

42. Yu Y, Shao W, Liu Y, Li Y, Zhong J, Ye H, Zhen L. Achieving high energy storage in BaTiO3/rGO/PVDF nanocomposites by regulating the charge transfer path at the hetero-interface. *J Mater Chem A*. **2023**;*11*:5279.

43. Han R, Wang L, Tang X, Qian J, Yu J, Chen X, Huang Y. Facile fabrication of rGO/LIG-based temperature sensor with high sensitivity. *Mater Lett*. **2021**;*304*:130637.

44. Khan T, Irfan MS, Ali M, Dong Y, Ramakrishna S, Umer R. Insights to low electrical percolation thresholds of carbon-based polypropylene nanocomposites. *Carbon*. **2021**;*176*:602.

45. Vieira LdS, dos Anjos EGR, Verginio GEA, Oyama IC, Braga NF, da Silva TF, Montagna LS, Passador FR. A review concerning the main factors that interfere in the electrical percolation threshold content of polymeric antistatic packaging with carbon fillers as antistatic agent. *Nano Select*. **2022**;*3*:248.

46. Kaur K, Jeet K. Electrical conductivity of water-based nanofluids prepared with graphene—carbon nanotube hybrid. *Fullerenes, Nanotubes, Carbon Nanostruct*. **2017**;*25*:726.

47. Sehrawat P, Islam SS, Mishra P. Reduced graphene oxide based temperature sensor: extraordinary performance governed by lattice dynamics assisted carrier transport. *Sens Actuators B Chem*. **2018**;*258*:424.

48. Guo F, Creighton M, Chen Y, Hurt R, Külaots I. Porous structures in stacked, crumpled and pillared graphene-based 3D materials. *Carbon*. **2014**;*66*:476.

49. Ma C, Xu J, Alvarado J, Qu B, Somerville J, Lee JY, Meng YS. Investigating the energy storage mechanism of SnS2-rGO composite anode for advanced Na-Ion batteries. *Chem Mater*. **2015**;*27*:5633.

50. Shi HH, Jang S, Naguib HE. Freestanding laser-assisted reduced graphene oxide microribbon textile electrode fabricated on a liquid surface for supercapacitors and breath sensors. *ACS Appl Mater Interfaces*. **2019**;*11*:27183.

51. Lipatov A, Varezhnikov A, Wilson P, Sysoev V, Kolmakov A, Sinitskii A. Highly selective gas sensor arrays based on thermally reduced graphene oxide. *Nanoscale*. **2013**;*5*:5426.

52. Tolvanen J, Hannu J, Jantunen H. Stretchable and washable strain sensor based on cracking structure for human motion monitoring. *Sci Rep*. **2018**;*8*:13241.

53. Eggers J, Villermaux E. Physics of liquid jets. *Rep Prog Phys*. **2008**;*71*: 036601.

54. Qu Y, Nguyen-Dang T, Page AG, Yan W, Das Gupta T, Rotaru GM, Rossi RM, Favrod VD, Bartolomei N, Sorin F. Superelastic multimaterial electronic and photonic fibers and devices via thermal drawing. *Adv Mater*. **2018**;*30*:e1707251.

55. Sordo F, Janecek E-R, Qu Y, Michaud V, Stellacci F, Engmann J, Wooster TJ, Sorin F. Microstructured fibers for the production of food. *Adv Mater*. **2019**;*31*:1807282.

56. Akhina H, Ramya KA, Gopinathan Nair MR, Saiter-Fourcin A, Garda MR, Deshpande AP, Kalarikkal N, Thomas S. Influence of reduced graphene oxide on flow behaviour, glass transition temperature and secondary crystallinity of plasticized poly(vinyl chloride). *RSC Adv*. **2020**;*10*:29247.

57. Brandrup J, Immergut EH, Grulke EA, Abe A, Bloch DR. Polymer handbook. New York: John Wiley & Sons, Inc; 1999.

58. Marsden AJ, Papageorgiou DG, Vallés C, Liscio A, Palermo V, Bissett MA, Young RJ, Kinloch IA. Electrical percolation in graphene–polymer composites. *2D Mater*. **2018**;*5*:032003.

59. Loh KP, Bao Q, Eda G, Chhowalla M. Graphene oxide as a chemically tunable platform for optical applications. *Nat Chem*. **2010**;*2*:1015.

60. Trung TQ, Le HS, Dang TML, Ju S, Park SY, Lee NE. Freestanding, fiber-based, wearable temperature sensor with tunable thermal index for healthcare monitoring. *Adv Healthc Mater*. **2018**;*7*: e1800074.

61. Nuthalapati S, Shirhatti V, Kedambaimoole V, Pandi NV, Takao H, Nayak MM, Rajanna K. Highly sensitive flexible strain and temperature sensors using solution processed graphene palladium nanocomposite. *Sens Actuators A Phys*. **2022**;*334*:113314.

Woo Mi Ryu obtained her B.S. degree in Chemical Engineering from University of Illinois Urbana-Champaign, Illinois, USA, in 2017, and M.S. degree in Bioengineering from Seoul National University, Seoul, Republic of Korea, in 2020. She is currently a Ph.D. student in Bio and Brain Engineering at Korea Advanced Institute of Science and Technology (KAIST), Daejeon, Republic of Korea under supervision of Professor Seongjun Park. Her research interests include the development of fiber-based translational biomedical devices and wearable electronics.

Geonho Park obtained his B.S. degree in Chemical and Biomolecular Engineering from Korea Advanced Institute of Science and Technology. He is currently a Ph.D. student in the Department of Nanoengineering at University of California, San Diego. His research interests include wearable sensors and translational diagnostic medical devices for telemedicine.

Yunheum Lee received the B.S degree in biomedical engineering from Sungkyunkwan University, Suwon, Republic of Korea, in 2021, and the M.S degree in bio and brain engineering from Korea Advanced Institute of Science and Technology (KAIST), Daejeon, Republic of Korea. He is currently a Ph.D. student from same department at the same university. His research interests include the development of fiber-based multifunctional devices and smart textile.

Seongjun Park received the B.S. degree in mechanical and aerospace engineering from Seoul National University, Seoul, Republic of Korea, in 2013, and the M.S. degree in mechanical engineering and Ph.D. degree in electrical engineering and computer science from Massachusetts Institute of Technology (MIT), Cambridge, MA, USA. He is currently an Assistant Professor with the Department of Bio and Brain Engineering, Korea Advanced Institute of Science and Technology (KAIST), Daejeon, Republish of Korea. He is also an adjunct professor in the Program of Brain and Cognitive Engineering, Graduate School of Green Growth and Sustainability, KAIST Institute for Health Science and Technology, KAIST Institute for NanoCentury, and the Center for Neuroscience-inspired Artificial Intelligence. His research interests include the development of soft material, fiber, or nanomaterial-based multifunctional biomedical and neural interfaces.

Yeonzu Son received the B.S. degree (summa cum laude) in biomedical engineering and electrical engineering from Ulsan National Institute of Science and Technology, Ulsan, Republic of Korea, in 2021. She is currently working toward the Ph.D. degree with the Program of Brain and Cognitive Engineering, Korea Advanced Institute of Science and Technology, Daejeon, Republic of Korea, working on biomedical and neural interface. Her academic interests include the development of biocompatible neural interface, with soft materials and nanoparticles, and wearable biomedical device for health-monitoring.